Scientific Research Publishing

Open Journal of Geology, 2026, 16(4), 157-170
https://www.scirp.org/journal/ojg
ISSN Online: 2161-7589
ISSN Print: 2161-7570

Methodological and Experimental Investigation of a Gravimetric Prospecting Technique Based on the Combined Exploitation of Smartphone Inertial Sensors

Abdoulaye Cissé[1,2], Ahmed Babacar Sarr[1,2], Sabou Sarr[1,2], Ndiouga Camara[2], Mapathé Ndiaye[1,2]

[1]Geophysics Laboratory, Iba Der Thiam University of Thiès, Thiès, Senegal
[2]Mechanics and Modeling Laboratory, University of Thiès, Thiès, Senegal
Email: abdoulaye.cisse87@univ-thies.sn

How to cite this paper: Cissé, A., Sarr, A.B., Sarr, S., Camara, N. and Ndiaye, M. (2026) Methodological and Experimental Investigation of a Gravimetric Prospecting Technique Based on the Combined Exploitation of Smartphone Inertial Sensors. *Open Journal of Geology*, **16**, 157-170.
https://doi.org/10.4236/ojg.2026.164009

Received: February 12, 2026
Accepted: March 24, 2026
Published: March 27, 2026

Abstract

Gravimetric surveying is widely used to detect subsurface density contrasts and to identify buried cavities and geological structures. Conventional gravimeters provide high precision but remain costly and complex. This study investigates a low-cost alternative based on the inertial sensors of a smartphone (iPhone 7), combining a tri-axial accelerometer and a gyroscope to estimate the local gravitational acceleration. The proposed method consists of performing repeated acceleration measurements, calibrating the sensors, correcting the device orientation through sensor fusion, and extracting the static component of gravity. Experiments were conducted under three configurations to evaluate repeatability and measurement precision. Processed data show standard deviations on the order of 10^{-6}, indicating good stability and reproducibility. These results demonstrate the feasibility of a portable and affordable gravimetric approach suitable for experimental and educational applications. Further validation against reference gravimeters is required to assess the metrological performance for geophysical exploration purposes.

Keywords

Geophysics, Gravimeter, Accelerometer, Gyroscope, Euler Angles, Density Contrasts, Measurement Precision

1. Introduction

Gravimetry is a reference geophysical technique for subsurface exploration and the characterization of lithological heterogeneities. Spatial and temporal varia-

tions in gravitational acceleration directly reflect density contrasts within the medium and therefore provide a valuable indirect proxy for buried structures such as tectonic discontinuities, cavities, or mineralized bodies [1]. The precise determination of the gravity field traditionally relies on absolute or relative gravimeters, as well as pendulum-based devices. However, these instruments remain constrained by high acquisition costs, complex logistics, and strict metrological requirements that limit their accessibility [2]. Although historically robust, pendulum methods exhibit strong sensitivity to uncertainties in mechanical parameters (effective length, friction, support instabilities, damping), generating systematic and random errors that may affect measurement reproducibility [3].

These technological constraints significantly restrict the availability of gravimetric instrumentation in many academic environments, particularly in resource-limited countries such as Senegal, where gravimetric experiments remain marginal in university settings.

Meanwhile, recent advances in microelectronics and MEMS technologies have enabled the integration of miniaturized tri-axial inertial sensors (accelerometers and gyroscopes) into smartphones. Originally designed for consumer applications, these sensors now achieve levels of resolution and stability compatible with certain high-precision physical measurements. Their low cost, portability, and widespread availability therefore offer a promising alternative for the development of lightweight and accessible gravimetric devices.

In this context, the present study proposes a methodology for determining local gravity intensity based on the quantitative exploitation of inertial measurements acquired from an iPhone 7 (Model A1778) running iOS XX. The approach relies on a processing chain including sensor calibration, instrumental noise characterization, filtering of dynamic components, and extraction of the gravitational component from the acceleration signal. The metrological performance of the system is evaluated through uncertainty and precision analyses. The signal-to-noise ratio (SNR) is used to assess the quality of the measurements recorded by the accelerometer.

The objective is to assess the feasibility of a low-cost gravimetric solution that could constitute a relevant alternative for experimental and educational applications.

2. Materials and Methods

2.1. Materials

The experimental setup is based on a rigid parallelepiped container with internal dimensions of 42 cm × 40 cm × 20 cm, specifically designed to accommodate the investigated granular media and to ensure controlled and repeatable measurement conditions. The container provides a stable mechanical support and a confined environment that minimizes external disturbances during acquisition (**Figure 1**).

It is successively filled with materials exhibiting contrasting physical properties,

including homogeneous dune sand and an irregularly shaped rock block. These materials were selected to generate different density distributions and mass configurations within the volume, thereby allowing assessment of the influence of bulk density contrasts and medium heterogeneity on the measured gravimetric response. This controlled substitution of materials enables a comparative analysis of gravity variations induced by subsurface mass changes under reproducible experimental conditions.

Figure 1. Experimental container (Author's own illustration).

2.2. Instrumentation

Inertial data acquisition is performed using a smartphone (iPhone 7) embedding an inertial measurement unit (IMU) based (MEMS) sensors, including a tri-axial accelerometer and a tri-axial gyroscope. These sensors provide simultaneous measurements of linear acceleration and angular velocity along three orthogonal axes.

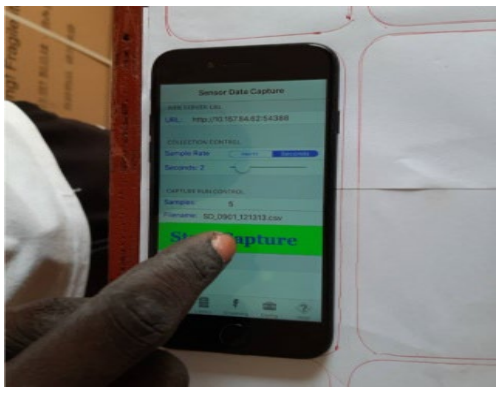

Figure 2. Experimental setup: smartphone on container using sensor data (author's own work).

Raw signals are recorded and stored using the Sensor Data application, downloaded from the App Store (https://apps.apple.com/app/sensor-data/id1457568621), which enables the extraction of acceleration and angular velocity components at a sampling frequency

adapted to the requirements of the study. This configuration ensures continuous data acquisition with sufficient temporal resolution for subsequent signal processing and gravity estimation.

All measurements were conducted with the smartphone positioned on the box, as illustrated in Figure 2.

The accelerometer measures the specific force applied to the smartphone, corresponding to the sum of dynamic accelerations and the mechanical reaction opposing gravity. When the device is perfectly stationary and horizontally aligned, the magnitude of the measured signal is equal to the gravitational acceleration g.

When the smartphone is in motion or tilted relative to the terrestrial reference frame, the accelerometer output a_{ac} corresponds to the sum of the projection of the gravity vector onto the sensor frame, the dynamic accelerations induced by the device's motion, and additional parasitic contributions arising from the sensor's intrinsic characteristics. Consequently, the measured acceleration can be expressed as:

$$a_{ac} = Rg + a_d + b$$

where:

- a_{ac} is the total acceleration measured by the accelerometer,
- g is the component associated with the Earth's gravitational acceleration,
- R is the attitude (rotation) matrix between the Earth frame and the sensor frame,
- a_d represents dynamic accelerations due to motion or misalignment of the device,
- b denotes sensor noise and bias.

After correcting for disturbing accelerations, knowledge of the Earth's gravity field provides valuable information about its internal structure and mass transfer processes [4]. Consequently, for geophysical prospecting purposes, only the gravitational component g is of interest.

Since the accelerometer measures the combined signal a_{ac}, a dedicated procedure is required to extract the gravitational contribution through orientation correction and filtering of dynamic components.

2.3. Attitude Estimation

The smartphone features a gyroscope measuring angular velocities $\left(\omega_x, \omega_y, \omega_z\right)$, which enables orientation estimation and projection of acceleration into the terrestrial frame. Orientation from low-cost inertial sensors is typically obtained via sensor fusion, combining the gyroscope's high-frequency response with the accelerometer's low-frequency stability to mitigate drift and noise. Common approaches include complementary filters, extended Kalman filters (EKF), and quaternion-based algorithms such as the Madgwick and Mahony filters. Smartphone motion is represented using Euler angles and attitude quaternions, with Euler's rotation theorem stating that any 3D rotation can be expressed as three successive rotations about the coordinate axes [5].

To analyze gyroscopic motion, this study adopts the classical sequence composed of precession, nutation, and spin (or proper rotation).

Precession corresponds to a rotation about the Z-axis through an angle ψ. During this motion, the Z-axis remains fixed, while the X and Y axes are transformed into the intermediate axes $(ox)_1$ and $(oy)_1$, respectively.

Nutation is then defined as a rotation about the axis $(ox)_1$ through an angle θ. As a result of this rotation, the axes $(oy)_1$ and $(oz)_1$ are transformed into the new axes $(oy)_2$ and $(oz)_2$, respectively.

Finally, the spin (or intrinsic rotation) occurs about the axis $(oz)_2$ through an angle ϕ.

By projecting these successive rotations onto the reference coordinate system, the corresponding rotation matrices are obtained.

The rotation matrix associated with the precession around the Z-axis is given by:

$$R_z(\psi)=\begin{pmatrix}\cos(\psi) & -\sin(\psi) & 1\\ \sin(\psi) & \cos(\psi) & 0\\ 1 & 0 & 0\end{pmatrix}$$

$$R_y(\theta)=\begin{pmatrix}1 & 0 & 0\\ 0 & \cos(\theta) & -\sin(\theta)\\ 0 & \sin(\theta) & \cos(\theta)\end{pmatrix},$$

$$R_x(\phi)=\begin{pmatrix}\cos(\phi) & 1 & -\sin(\phi)\\ 0 & 0 & 0\\ \sin(\phi) & 0 & \cos(\phi)\end{pmatrix}$$

The successive combination of the three rotations through matrix multiplication results in a 3 × 3 matrix, referred to as the attitude matrix, which describes the transformation between the body frame and the reference frame:

$$R=R_z(\psi)R_y(\theta)R_x(\phi)$$

where $R_z(\psi), R_y(\theta)$ and $R_x(\phi)$ denote the rotation matrices associated with precession, nutation, and spin, respectively.

The attitude quaternion q provides a simpler way to express the attitude matrix. A quaternion mathematically represents a rotation of angle θ (in radians) about a unit vector $u(i,j,k)$.

Mathematically, the attitude quaternion can be written as:

$$q=q_1+q_2i+q_3j+q_4k$$

$i*j=k$, $j*i=-k$, $j*k=i$, $k*j=-i$, $k*i=j$, $i*k=-j$;
$i*i=j*j=k*k=-1$

2.4. Sensor Calibration

To reduce systematic errors, a static six-position calibration $(\pm X,\pm Y,\pm Z)$ is performed prior to each measurement series.

This procedure allows the estimation of:

- offset bias,
- scale factor.

The resulting calibration parameters are subsequently applied to correct all acquired measurements.

The acceleration measured along the vertical axis should be $\pm g \approx 9.81\,\mathrm{m/s^2}$.

For each axis i, the scale factor s_i and bias b_i of the accelerometer are given by:

$$s_i = \frac{2g}{a_{i+} - a_{i-}};\ b_i = \frac{a_{i+} - a_{i-}}{2}$$

where a_{i+} and a_{i-} are the measured accelerations for the positive and negative orientations [6] [7] of axis i. Then:

$$a_{Z,corrected} = s_Z \cdot \left(a_Z - b_Z\right)$$

For gyroscope, the bias is given by:

$$b_i = \frac{1}{N}\sum_{k=1}^{N} \omega_i[k]$$

$$\omega_{i,corrected} = \left(a_i - b_i\right)$$

A simple Excel spreadsheet can be used to correct the raw measurements by applying the calculated scale factors and biases for each axis.

3. Experimental Protocol

In a first step, the experimental container is kept empty. Under this configuration, thirteen independent acquisitions of the total acceleration are performed using the *Sensor Data* application in order to establish a reference condition.

In a second step, the container is completely filled with homogeneous dune sand. Thirteen additional measurements are then carried out following the same experimental protocol to ensure data comparability.

Finally, a third configuration is considered by introducing an irregularly shaped rock block with a lower mass than the previously used sand. A final measurement series is conducted under identical conditions.

Accelerometer measurements are subsequently corrected using the calibration parameters and inertial data fusion based on orientation information provided by the gyroscope. This procedure compensates for device tilt effects and sensor bias and enables extraction of the static gravitational component.

All acquisitions are performed at a frequency of 100 Hz, at the same location, during a single experimental session, and under identical environmental conditions in order to minimize external biases and ensure measurement reproducibility. For each acquisition, five consecutive acceleration values are recorded over a five-second interval. Their temporal average is then computed to reduce random noise. After correction and averaging, thirteen mean values of the static gravitational acceleration are obtained for each experimental configuration.

The smartphone position is referenced within an orthonormal (x, y) coordinate system defined on the container, enabling precise spatial localization of measurement points.

4. Gravity Reference and Validation Procedure

To strengthen validation of the experimental protocol, the mean values of the measured relative gravity after correction and statistical processing are converted to absolute gravity and compared with the theoretical gravity expected at the measurement location. This comparison allows evaluation of the consistency and reliability of the gravity estimates derived from the inertial sensors.

The theoretical normal gravity at the surface of the reference ellipsoid is calculated using the international WGS-84/IGSN formula:

$$g(\phi) = 9.780327\left(1 + 0.0053024\sin^2\phi - 0.0000058\sin^2(2\phi)\right)$$

where ϕ is the geodetic latitude. The altitude effect is then accounted for using the free-air correction:

$$g_{th} = g(\phi) - 3.086\times10^{-6}h$$

where h is the altitude in meters.

Absolute gravity is finally estimated by normalization of the measured gravity with respect to the theoretical reference value [8] [9]:

$$g_{abs} = g_{mes} \times \frac{g_{th}}{g_{ref}}$$

where g_{mes} denotes the corrected experimental gravity and g_{ref} the reference value obtained during calibration with the empty container. The relative error is defined as $\varepsilon = \frac{\Delta_g}{g_{th}}$ with $\Delta_g = g_{abs} - g_{th}$.

In gravimetry, $1\,\text{mGal} = 10^{-5}\,\text{m/s}^2$. For n measurements, the uncertainty of the mean gravity value is given by

$$u = \frac{\sigma_g}{\sqrt{n}}$$

where σ_g is the standard deviation of the measurements.

The signal-to-noise ratio (SNR) is used as a performance indicator to assess the detectability of gravity anomalies relative to the intrinsic sensor noise [10]. It provides a quantitative measure of measurement reliability and enables evaluation of the instrumental sensitivity and stability of the proposed smartphone-based gravimetric system

$$\text{SNR} = \frac{\Delta_g}{u}$$

5. Results and Discussion

5.1. Data Presentation

Table 1 presents the bias and scale factor values obtained after sensor calibration.

Table 1. Estimated bias and scale factor.

Configurations	Bias b (g)	Scale factor s
Configuration 1	1.7×10^{-3}	**0.9996**
Configuration 2	-1.9×10^{-3}	**1.0007**
Configuration 3	1.2×10^{-3}	**0.9999**

The following section presents the results obtained from the experimental measurements carried out under the three configurations described above.

5.1.1. Results for the Empty Container (Reference Condition)

The mean value of the measured relative gravity $\overline{g}$ correspond to the component of g along the measurement axis Z, and the corresponding standard deviation σ_g are:

$$\overline{g} = -0.99992415\,; \quad \sigma_g = 2.15512 \times 10^{-6}$$

After conversion to physical units and uncertainty estimation, the results become:

$$\overline{g} = 9.80925591\ \mathrm{m/s^2}, \quad g = \overline{g} \pm 0.59\ \mathrm{mGal} \quad \text{and}$$

$$\sigma_g = 2.1147\ \mathrm{mGal}$$

The geodetic latitude of Thiès is $\phi = 14.7894^\circ$, and the mean altitude is 63 m. The corrected theoretical gravity is therefore:

$$g_{th} = 9.78370 - 0.00019 = 9.78351\ \mathrm{m/s^2}$$

5.1.2. Results for the Container Filled with Dune Sand

The mean relative gravity and standard deviation are:

$$\overline{g} = -0.999925938; \quad \sigma_g = 1.7357 \times 10^{-6}$$

The standard uncertainty of the mean for ($n = 13$) measurements is:
$u = 0.47$ mGal , corresponding to ±0.94 mGal at the 95% confidence level.

After conversion and correction, the absolute gravity and standard deviation are:

$$g_{abs} = 9.7835275\ \mathrm{m/s^2}\,; \quad \sigma_g = 1.73\ \mathrm{mGal}$$

$$\Delta_g = 0.0000175\ \mathrm{m/s^2} = 1.75\ \mathrm{mGal}$$

$$\mathrm{SNR} = 3.72; \quad \varepsilon = 1.8 \times 10^{-6}$$

5.1.3. Results for the Container Containing a Rock Block

The mean relative gravity and standard deviation are:

$$\overline{g} = -0.99992575\,; \quad \sigma_g = 1.50756 \times 10^{-6}$$

After conversion and uncertainty estimation:

$$g = 980.925\ \mathrm{mGal} \pm 0.41\ \mathrm{mGal}$$

$$g_{abs} = 9.7835257\ \mathrm{m/s^2}\,; \quad \Delta_g = 1.57\ \mathrm{mGal}$$

$$\sigma_g = 1.48\ \mathrm{mGal}$$

$$\text{SNR} = 4.88\,; \quad \varepsilon = 1.60\times10^{-6}$$

5.2. Data Processing and Interpolation

Following acquisition, the processed gravity values are imported into SURFER 18 softwares to generate spatial distribution maps. Interpolation is performed using the natural neighbor method, which ensures smooth and physically consistent spatial reconstruction without introducing artificial extrema.

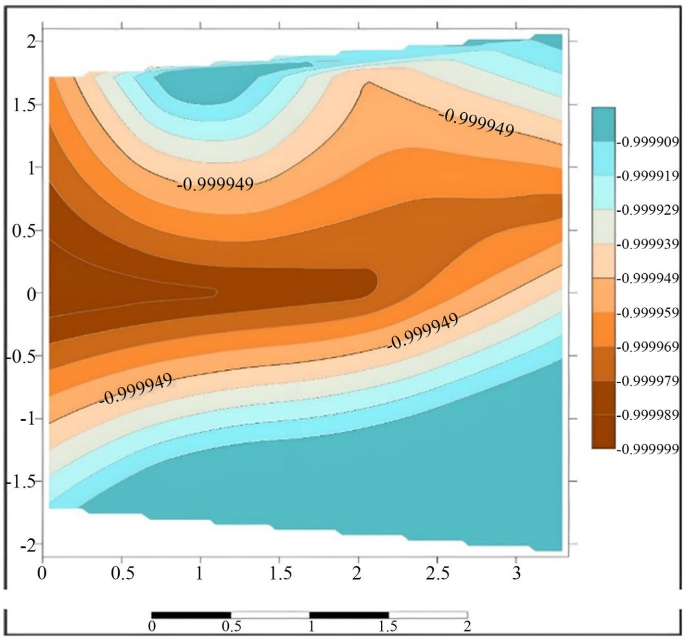

Figure 3. Spatial distribution map of *g* values (Empty container).

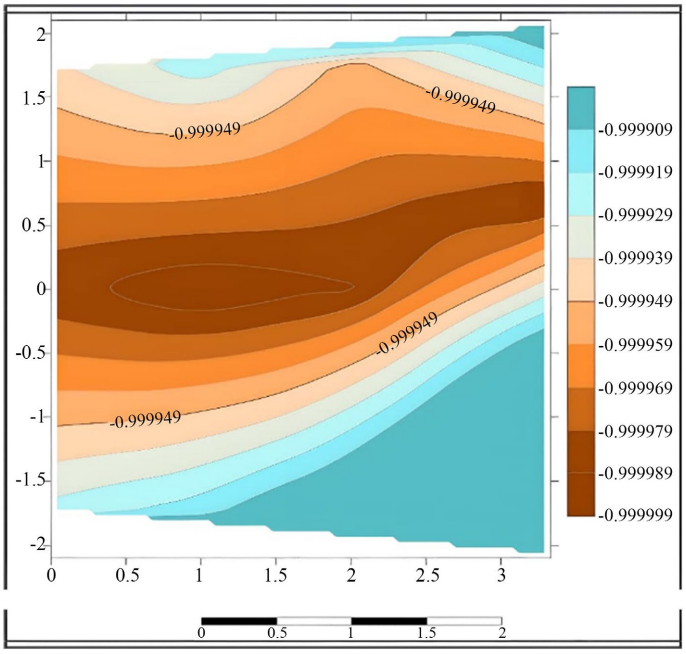

Figure 4. Spatial distribution map of *g* values (Container with rock block).

The resulting maps illustrate the spatial distribution of gravity variations (Figures 3-5) and facilitate visualization of density contrasts induced by the different materials.

The maps were generated using a reference grid drawn on the box to precisely indicate the smartphone's position during each measurement. In this coordinate system, the vertical axis represents the ordinate, while the horizontal axis represents the abscissa.

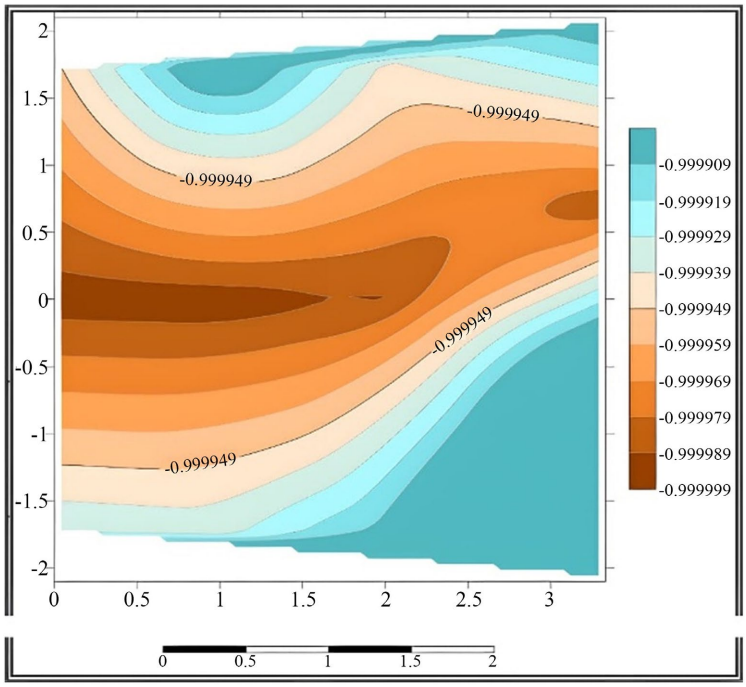

Figure 5. Spatial distribution map of g values (Container with dune sand).

5.2.1. Interpretation and Discussion of the Measured Gravity Values

The measurements obtained with the empty container serve as the reference state of the local gravitational field. The normalized mean value is

$$\overline{g} = -0.99992415$$

with a very low standard deviation $\sigma_g = 2.16 \times 10^{-6}$, indicating excellent sensor stability and minimal instrumental noise. After conversion to physical units, the local theoretical gravity—calculated from the geodetic latitude of Thiès (14,7894°) and corrected for the mean altitude (63 m) is

$$g_{th} = 9.78351 \text{ m/s}^2$$

This value serves as the reference for evaluating the subsequent experimental configurations. The small dispersion of the measurements confirms the high repeatability of the acquisition protocol and validates the use of a smartphone as a relative gravimetric sensor.

With the introduction of dune sand, the measured mean absolute gravity becomes $g_{abs} = 9.7835275 \text{ m/s}^2$, corresponding to a variation of $\Delta_g = 1.75$ mGal; $\varepsilon = 1.8 \times 10^{-6}$

The standard deviation decreases to $\sigma_g = 1.71$ mGal indicating improved mechanical stability of the system. This reduction in noise can be attributed to the damping effect of the sand, which limits micro-vibrations and enhances signal quality.

The observed increase in gravity, though small, is consistent with the presence of additional mass near the sensor, in accordance with Newtonian gravitational attraction. The order of magnitude (a few mGal) matches the expected gravimetric anomalies for small-scale local density variations. The anomaly is approximately 3.7 times larger than the measurement noise, making it clearly detectable.

In the final configuration (container with a rock block), the measured gravity is

$$g_{abs} = 9.7835257 \text{ m/s}^2;$$

$$\Delta_g = 1.57 \text{ mGal}; \quad \varepsilon = 1.60 \times 10^{-6}.$$

The standard deviation further decreases to $\sigma_g \approx 1.48$ mGal, indicating the highest repeatability among the three tests. The slightly smaller gravity variation compared to the sand configuration can be explained by the lower mass of the rock block relative to the dune sand, as well as its geometry and spatial distribution within the container. The signal-to-noise ratio of 4.88 demonstrates strong statistical significance, confirming that the observed anomalies are reliably detectable.

5.2.2. Interpolation of Standard Deviations

The maps below (**Figures 6-8**) show the standard deviations of the static gravitational acceleration obtained after data processing and interpolation. The spatial distribution of the measurement variability was reconstructed to visualize regions of higher or lower instrumental dispersion. Interpolation was performed using the natural neighbor method, ensuring smooth transitions between measurement points while preserving the local characteristics of the data.

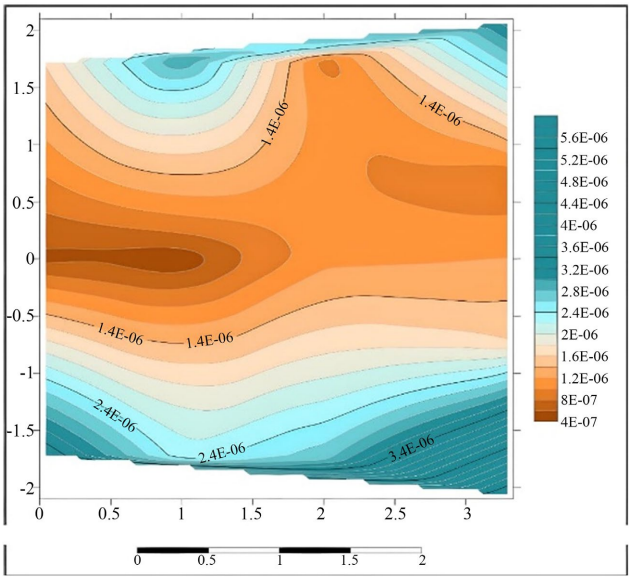

Figure 6. Standard deviation Map of *g* measurements (Empty container).

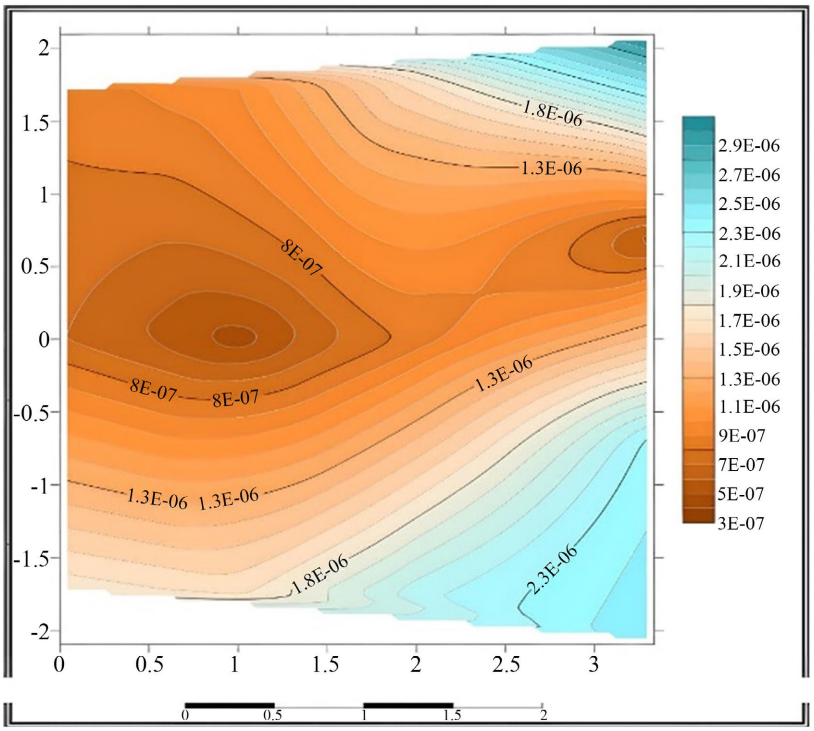

Figure 7. Standard deviation map of *g* measurements (Container with rock block).

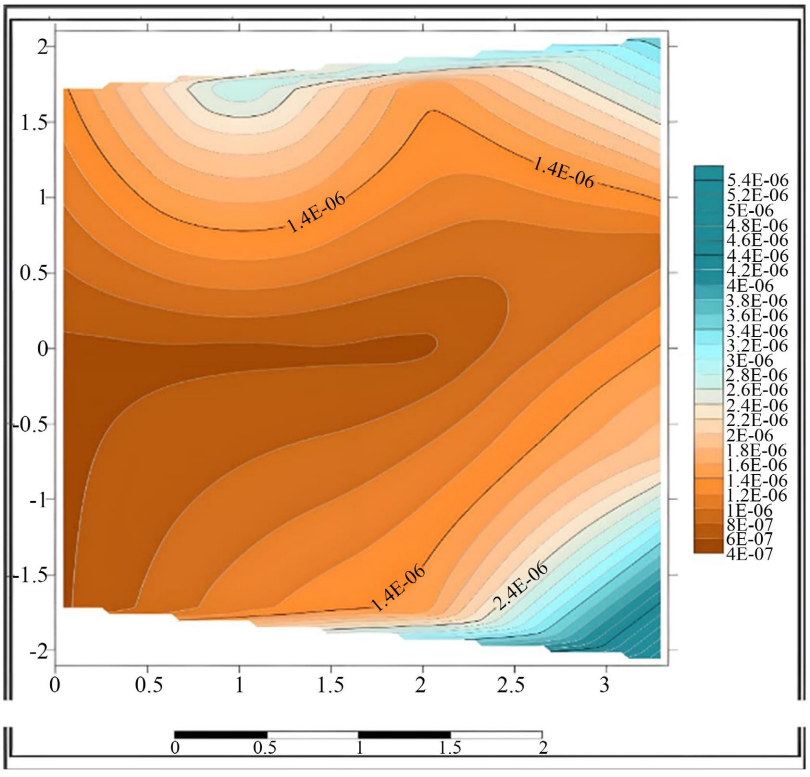

Figure 8. Standard deviation map of *g* measurements (Container with dune sand).

5.2.3. Discussion on the Standard Deviation Values

The analysis of standard deviations reveals a progressive decrease in measurement

dispersion across the different configurations. The empty container exhibits the highest standard deviation ($\sigma = 2.16 \times 10^{-6}$), although this value remains very low, indicating excellent sensor stability and high measurement repeatability. Filling the container with dune sand results in a reduced standard deviation (1.74×10^{-6}), suggesting a mechanical damping effect of the granular material. This trend is further confirmed with the rock block configuration, for which the standard deviation reaches its minimum (1.51×10^{-6}), indicating improved local coherence of the measurements despite the presence of a more localized gravimetric anomaly. These observations highlight the influence of material properties on the stability and dispersion of gravimetric measurements.

These results demonstrate the potential of the measurement system, considering that uncertainties in relative gravimeters typically range around $10^{-8} g$ for high-precision spring gravimeters and $10^{-9} g$ for superconducting gravimeters [2].

It should be noted that the directly measured gravity values are relative; they are suitable for exploration geophysics but must be calibrated against sites with known absolute gravity or corrected relative to a base station. Calibration consists in determining the proportional relationship between device readings and gravity variations, which is generally linear.

Overall, this study shows that gravimetric measurements based on a high-resolution accelerometer can discriminate between different material configurations in a controlled setting. The results are particularly relevant for geotechnical reconnaissance, notably for identifying density variations associated with lithological changes, fill zones, or subsurface voids. In perspective, the developed approach could be adapted to the detection of shallow buried structures (cavities, foundations, networks) as a complement to conventional geophysical methods.

6. Conclusions

The processing and analysis of the acquired gravimetric data validated the consistency and robustness of the proposed experimental protocol. The methodology is based on recording total acceleration using the smartphone accelerometer, combined with orientation correction derived from gyroscope measurements. The use of kinematic modeling based on Euler angles and quaternion representation of the device attitude allowed reliable extraction of the static gravitational component from the inertial signal.

The experimental performance demonstrates excellent instrumental precision, with dispersions on the order of $10^{-5} g$. The measurements reveal detectable gravimetric anomalies depending on the material, as well as a coherent relationship between the increase in the container's bulk density and the measured local gravity variation. The very low relative error (<2 ppm) compared to the theoretical value confirms the metrological validity of the protocol.

These results demonstrate that smartphone-embedded inertial sensors can detect small density contrasts and highlight their potential as a simple, portable, and

cost-effective alternative for experimental and educational applications. This approach opens promising perspectives for low-cost geophysical prospecting, particularly for the reconnaissance of near-surface structures, lithological heterogeneities, or buried cavities. Future work focusing on fine sensor calibration, improved spatial resolution, and integration with gravimetric inversion methods will enhance the reliability and operational potential of this methodology.

Conflicts of Interest

The authors declare no conflicts of interest regarding the publication of this paper.

References

[1] Merlet, S. (2010) Détermination absolue de g dans le cadre de l'expérience de la balance du watt.

[2] Bonvalot, S. (2010) Ecole d'été 2010 du GRGS—Mesures et traitement de gravimétrie terrestre.

[3] Ducarme, B. (1972) La détermination du champ de la pesanteur.

[4] Torge, W. (1989) Gravimetry. Walter de Gruyter.

[5] Luiza, M. and Vianna, C. (2018) Calcul de l'Angle de Dérive d'un Véhicule basé sur le Filtre de Kalman.

[6] Shin, E.H. and El-Sheimy, N. (2002) New Calibration Method for Strapdown Inertial Navigation Systems. *Journal of Geodesy*, **127**, 41-50.

[7] Visser, P. (2009) GOCE Gradiometer: Estimation of Biases and Scale Factors of All Six Individual Accelerometers by Precise Orbit Determination. *Journal of Geodesy*, **83**, 69-85. https://doi.org/10.1007/s00190-008-0235-8

[8] Sokolov, A.V., Krasnov, A.A., Kuz'mina, N.V. and Stus', Y.F. (2022) Measurement of Absolute Gravity and Deflections of the Vertical at Sea. In: *International Association of Geodesy Symposia*, Springer, 3-13. https://doi.org/10.1007/1345_2022_140

[9] Sobrero, F.S., Ahlgren, K., Bevis, M.G., *et al.* (2024) A Robust Approach to Terrestrial Relative Gravity Measurements and Adjustment of Gravity Networks. *Journal of Geodesy*, **98**, Article No. 86. https://doi.org/10.1007/s00190-024-01891-w

[10] Hines, A., Nelson, A., Zhang, Y., Valdes, G., Sanjuan, J., Stoddart, J. and Guzmán, F. (2022) Optomechanical Accelerometers for Geodesy. *Remote Sensing*, **14**, Article 4389. https://doi.org/10.3390/rs14174389